

Chapter 2

Effect of Strain Rate and Interface Chemistry on Failure in Energetic Materials

Chandra Prakash, I. Emre Gunduz, and Vikas Tomar

Abstract We study the failure at interfaces between Hydroxyl-terminated polybutadiene (HTPB)-Ammonium Perchlorate (AP) based energetic material. In this work, interface mechanical strength of a set of HTPB-AP interfaces is characterized using nano-scale impact experiments at strain rates up to 100 s^{-1} . A power law viscoplastic constitutive model was fitted to experimental stress-strain-strain rate data in order to obtain constitutive behavior of interfaces, particle, and matrix. A mechanical Raman spectroscopy is used to analyze the effect of binding agent at different temperature. A tensile fracture experiment combined with In-situ Mechanical Raman Spectroscopy was used to obtain fracture properties. Stress maps are obtained near the interface using In-situ Mechanical Raman Spectroscopy to analyze the changes in the stress distribution around interfaces for different loads till failure. Cohesive zone model parameters were obtained from the consideration of local stress during failure and the cohesive energy required for delamination of AP from HTPB matrix. Effect of binding agent on the interface strength is found to be quite significant. The cohesive zone parameters and the viscoplastic model obtained from the experiment were then used in the cohesive finite element method to simulate the dynamic crack propagation as well as the delamination. Results show that interfacial properties are affected by the rate of loading and are also dependent upon the binding agent.

Keywords Energetic material • Stress/strain relationship • HTPB • AP • NRS

Energetic compounds are employed in a large number of applications, such as, explosive, propellant, and pyrotechnic formulations. An example of a heterogeneous solid propellant used in rocket industry is a crystalline oxidizer (e.g., ammonium perchlorate-AP) embedded in a polymeric binder (e.g., Hydroxyl-Terminated Polybutadiene or HTPB). Aluminum (Al) particles are sometimes added to enhance the propellant performance. A typical industrial solid propellant consists of 70% AP, 10% HTPB and around 20% Al by weight, [1]. Three main failure mechanisms in the composite material are identified as particle fracture, interfacial failure and the cavitation in the binder [2]. Palmer [2] investigated a number of polymer bonded explosives (PBXs) under tensile loading and observed finding a wide range of responses. They found that the crack propagation was mostly confined to binder and that the interface debonding was the dominant failure mode. Interface strength depends on the constituent material, i.e., particle, matrix and/or binding agents [3, 4].

Several experiments [5–7] have suggested a particle size effect on the performance of energetic materials. Yeager [8] has shown the effect of interface/interphase and the microstructure on the mechanical behavior of PBXs. Interfacial structure was altered by adding a plasticizer in the composite. The plasticizer was shown to inhibit the formation of a large interface/interphase and was more likely to have film delamination than the no-plasticized composite. The difference in interfacial properties was also shown to have significant effect on the crack initiation and explosive sensitivity.

Two samples were prepared for analyzing the effect of functionalization on the interface mechanical properties. One consist of ammonium perchlorate (AP) particles embedded in hydroxyl-terminated polybutadiene (HTPB). In the second sample, a surface binding agent (Tepanol) was added at a mass ratio of 0.5 to fabricate samples with higher surface adhesion, while keeping the same index ratio.

C. Prakash • V. Tomar (✉)

School of Aeronautics and Astronautics, Purdue University, West Lafayette, IN, 47907, USA
e-mail: cprakash@purdue.edu; tomar@purdue.edu

I. Emre Gunduz

School of Mechanical Engineering, Purdue University, West Lafayette, IN, 47907, USA

Table 2.1 Viscoelastic material parameters for AP, HTPB and the HTPB/AP interface

	χ (MPa) ⁻ⁿ		m		n	
	Sample-1	Sample-2	Sample-1	Sample-2	Sample-1	Sample-2
HTPB	25.52	13.13	-19	-13	25	30
AP	18	19.9	-16	-17	9	9
HTPB/AP interface	40.3	12.8	-30	-10	8	3

Energetic materials have been modeled using viscoelastic [9, 10] as well as elasto-viscoplastic [11, 12] model. For high strain rate loading viscoplastic models are used frequently [13–15]. Kalayciogly [12] et al. modeled an HTPB/AP composite propellant using Perzyna's viscoplastic model. In this work, following Tsai and Sun, [16], we assume an effective stress-effective viscoplastic strain curve by a power law model

$$\bar{\varepsilon}^{vp} = A(\bar{\sigma})^n, \quad (2.1)$$

where $\bar{\varepsilon}^{vp}$ and $\bar{\sigma}$ are the equivalent strain and equivalent stress respectively. A is a power law function of effective plastic strain rate given as,

$$A = \chi \left(\dot{\bar{\varepsilon}}^0 \right)^m. \quad (2.2)$$

The viscoplastic model then can be given as,

$$\dot{\bar{\varepsilon}}^{vp} = \chi \left(\dot{\bar{\varepsilon}}^0 \right)^m (\bar{\sigma})^n. \quad (2.3)$$

The values of χ , m and n are found from the stress strain data obtained during nano-scale impact test, [17].

Mechanical properties were obtained using a nano-scale impact experiment. The experimental procedure involves impacting the surface of material being tested by an indenter. The nano-scale impact were performed using the high strain rate impact schedule of Micro Materials, UK [18–21].

Table 2.1 shows that the viscoplastic model parameters for the interface, the matrix (HTPB) and the particle (AP) for two samples. These material parameters then further can be used to describe the material behavior at the interface as well as in the matrix and particle phase for high strain rates. The present analysis shows nano-scale impact as a tool to capture the material deformation behavior at micrometer scales.

As shown in Fig. 2.1a, the samples were loaded in tension at a loading rate of 0.1 mm/min till fracture. During the loading, a set of points on the sample near interface was scanned to get Raman shifts, [22]. These Raman shifts were obtained at different loads until the debonding occurred. The strength of the interface was evaluated from the stress map obtained using Raman spectroscopy by assuming the strength equal to the stress at the start of the delamination. The strength of the interface is the stress near the interface at the load during failure (Fig. 2.1b). Area under the load displacement curve, Fig. 2.1c, between the point where crack reaches the interface and the point where interface delaminates is the total energy required for delamination.

The dynamic behavior of the composite material system is modeled using the explicit finite element method (see e.g., [23, 24]). The average time step is of the order of 1 ns which is approximately one tenth of the time it takes for the longitudinal wave to traverse the smallest bulk element in the meshes in current research. The weak form of the governing equation is given as,

$$\int_V \tau : \delta \mathbf{F} dV - \int_{S_{int}} \mathbf{T} \cdot \delta \mathbf{\Delta} dS = \int_{S_{ext}} \mathbf{T} \cdot \delta \mathbf{u} dS - \int_V \rho \frac{\partial^2 \mathbf{u}}{\partial t^2} \cdot \delta \mathbf{u} dV, \quad (2.4)$$

To track complex crack/microcrack patterns, arbitrary crack paths, and crack branching, cohesive surfaces are specified along all finite element boundaries as an intrinsic part of the finite element model. The finite element meshes used have a uniform structure with “cross-triangle” elements of equal dimensions arranged in a quadrilateral pattern, Fig. 2.2. This type of triangulation is used since it gives the maximum flexibility for resolving crack extensions and arbitrary fracture patterns [25].

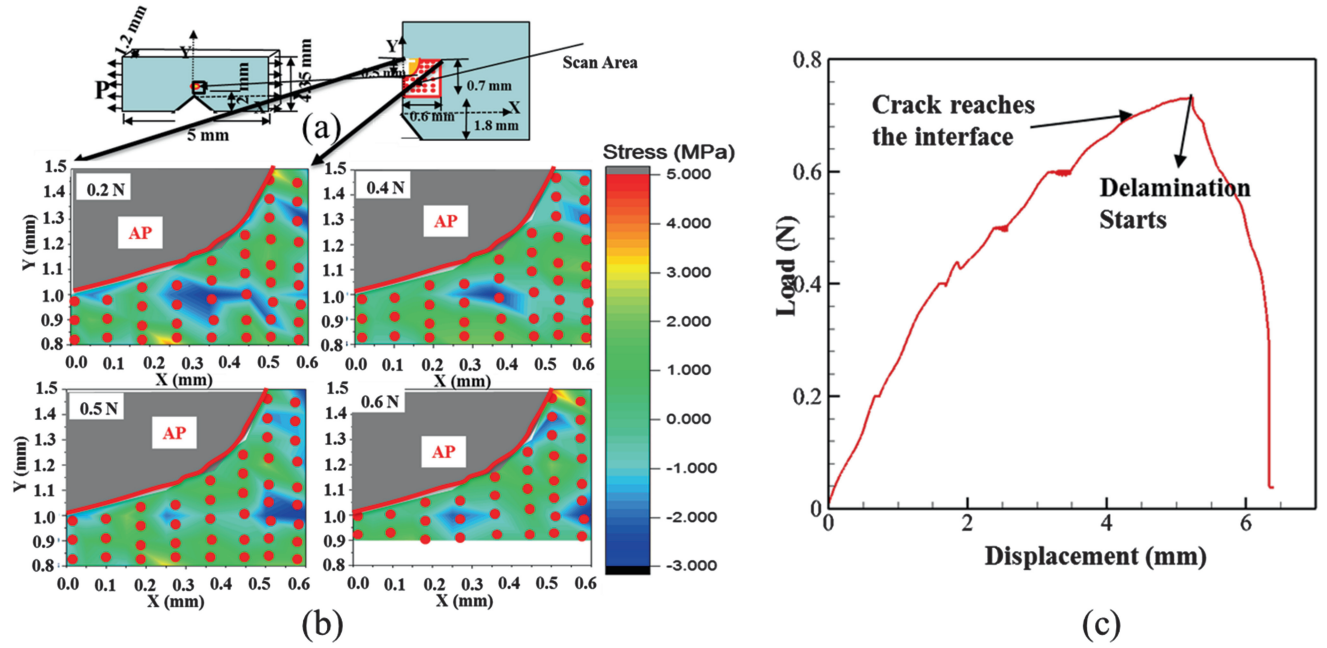


Fig. 2.1 (a) Loading configuration, (b) stress distribution around the interface for different load until failure and (c) Load-displacement curve

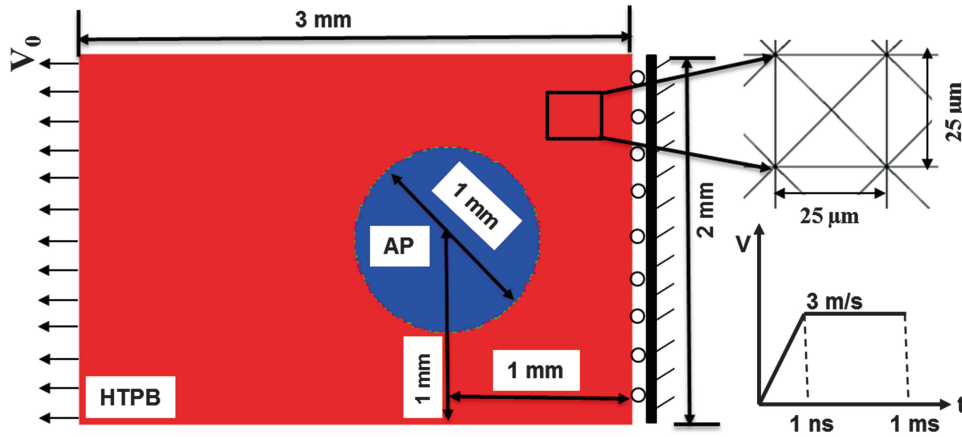


Fig. 2.2 Finite element mesh of the energetic material model being studied

We use the standard assumption for finite strain inelastic problems: the multiplicative decomposition of the deformation gradient F into an elastic and an inelastic part F^e and F^p , i.e.,

$$F = F^e \cdot F^{vp} \quad (2.5)$$

In the cohesive model used, the traction T applied on material points coinciding at and occupying position x on cohesive surface in the reference configuration is work-conjugate to surface separation Δ . Reckoned in the reference configuration, the cohesive law is

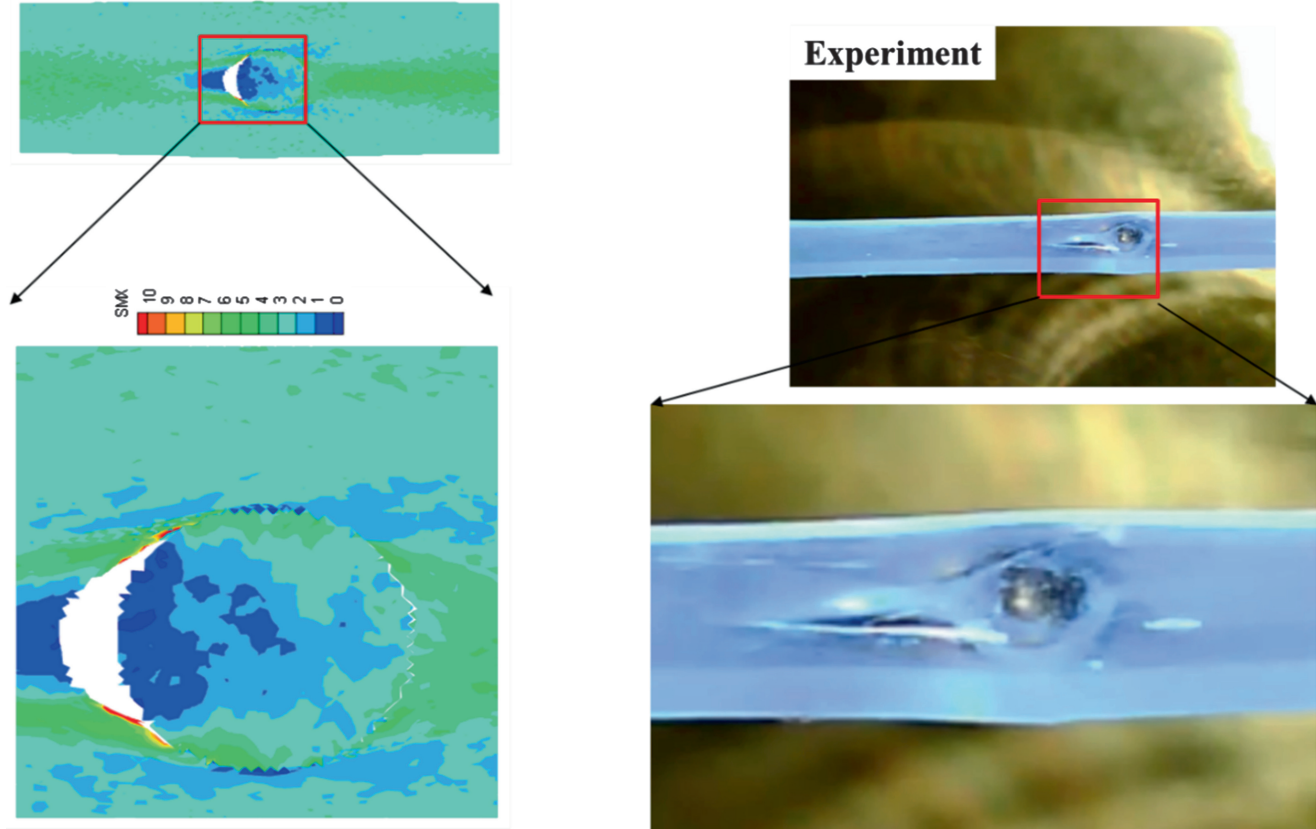
$$T(x) = T[\Delta(x)], \quad (2.6)$$

and the work of separation under this traction at any stage of deformation is [26],

$$W_{sep} = \int_{S_0} \int_0^\Delta T(x, \Delta) . d\Delta dx. \quad (2.7)$$

Table 2.2 Cohesive zone parameters for constituents of HTPB/AP composite

Material/interface	Cohesive strength (MPa)	Critical displacement (mm)	Cohesive energy (N/mm)
HTPB	0.8	0.5	0.2
AP	200	1×10^{-6}	1×10^{-4}
Interface	0.5–6	0.11	0.02–0.33

**Fig. 2.3** Validation of delamination mode obtained using CFEM with experiment

The CFEM simulations are carried out under plane strain assumption. The plane strain assumption is therefore a major limitation of the framework. The irreversible bilinear law is used which is a generalized version of the cohesive laws with irreversibility [27, 28]. The current law is derived from a description ϕ of the surface energy dissipation per unit area which is a function of separation vector Δ through a state variable defined as that describes the effective instantaneous state of mixed-mode separations. The specific form for ϕ is taken as, [29].

A two dimensional numerical simulation is carried out for the AP-HTPB specimen with a single AP particle embedded in HTPB binder to simulate the failure. Figure 2.1 illustrates the geometry and boundary conditions employed in the numerical simulation. The AP particle is idealized as a circle with diameter $D = 1$ mm. The size of the element was chosen such that it satisfies the bounds given in [30], which is equal to $25 \mu\text{m}$.

Local cohesive zone parameters used in the simulation were obtained from the Raman spectroscopy experiment, [17], and are given in Table 2.2. These parameters for HTPB and HTPB/AP interface were obtained from the Raman spectroscopy as explained above. For AP the cohesive strength is assumed to be $E/100$, [30], where E is the Young's modulus of AP. HTPB/AP interface cohesive strength was varied to study the effect of different interface. Figure 2.3 shows the similarity in the mode of delamination observed in both numerical and experimental observations.

Strain rates of 100, 200, 800, 1000, 2000, 3000 s^{-1} were applied in terms of the velocity boundary condition at the top boundary. Figure 2.4a shows the effect of strain rates on the cohesive energy of the system. Cohesive energy increases with the time as the deformation increases, even when the cohesive zone parameters are constant. This is because the material model used is a rate dependent viscoplastic material. The rate at which the cohesive energy increases also increase with strain rate. Delamination starts near the fix boundary at low strain rates (800 s^{-1} and 1000 s^{-1}). However, as the strain

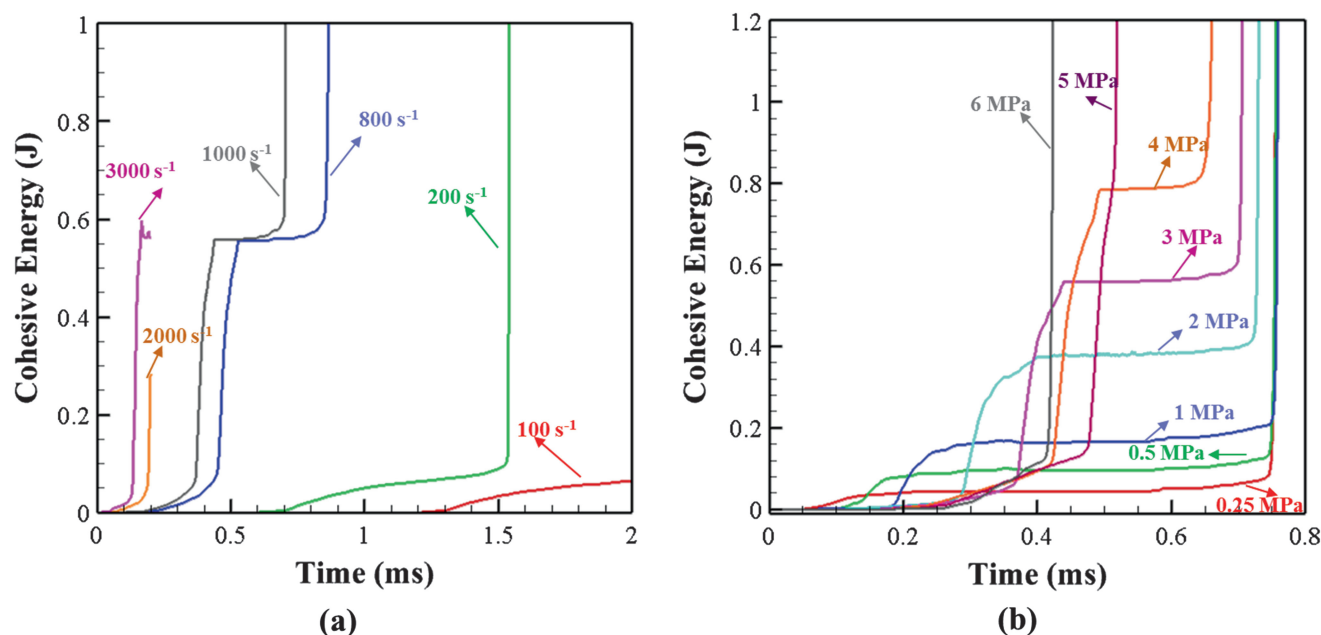


Fig. 2.4 Cohesive energy of the system (a) for different strain rates and (b) for different cohesive strength with time

rate increases the delamination occurs on the loading side (3000 s⁻¹). Figure 2.4b shows the effect of cohesive strength on the cohesive energy. The delamination occurs when the cohesive energy reaches the critical value. As can be seen in the Fig. 2.4b, time at which cohesive energy reaches its critical value, decreases with increasing cohesive strength.

This work shows the effect of interface strength and the strain rate on the debonding in HTPB/AP composite. We obtain a strain rate dependent mechanical properties of constituents of the HTPB/AP composite using a nano-scale impact experiment which allows us to obtain not only the properties of constituents but also of interface which is otherwise difficult to obtain. Cohesive parameters based on in-situ mechanical Raman spectroscopy based on change in interface chemistry by adding a binding agent into the composite propellant. We then use these experimentally obtained properties into our cohesive finite element model (CFEM) to simulate the delamination of HTPB-AP interface. The dynamic fracture behavior is simulated for the HTPB/AP sample with CFEM. The CFEM simulation accurately captures the evolution and mode of delamination. This has been confirmed by comparing it with the quasi-static tensile experiment also. Strain rate effects are considered and shown to affect the delamination in the sample. The effect of interface chemistry on delamination mode can eventually effect the possible hot-spots in the material. Further study would be needed to quantify this effect in multi-particle energetic materials.

Acknowledgments This research was supported by US-AFoSR Grant FA9550-15-1-0202 (Program Manager Dr. Martin Schmidt).

References

- Gallier, S., Hiernard, F.: Microstructure of composite propellants using simulated packings and X-ray tomography. *J. Propuls. Power.* **24**(1), 154–157 (2008)
- Palmer, S.J.P., Field, J.E., Huntley, J.M.: Deformation, strengths and strains to failure of polymer bonded explosives. *Proc. R. Soc. A: Math. Phys. Eng. Sci.* **440**, 399–419 (1993)
- Stacer, R.G., Hubner, C., Husband, M.: Binder/filler interaction and the nonlinear behavior of highly-filled elastomers. *Rubber Chem. Technol.* **63**(4), 488–502 (1990)
- Stacer, R.G., Husband, M.: Small deformation viscoelastic response of gum and highly filled elastomers. *Rheol. Acta.* **29**, 152–162 (1990)
- Fleming, K.A., et al.: The influence of formulation variables on the growth of reaction in plastic bonded explosives. In: *Proceedings of the 8th International Detonation Symposium*, Albuquerque. Naval Surface Weapons Center (1985)
- Kimura, E., Oyumi, Y.: Shock instability test for azide polymer propellants. *J. Energ. Mater.* **16**(2–3), 173–185 (1998)
- Rae, P.J., et al.: Quasi-static studies of the deformation and failure of β -HMX based polymer bonded explosives. *Proc. R. Soc. A: Math. Phys. Eng. Sci.* **458**, 743–762 (2002)
- Yeager, J.D.: *Microstructural Characterization of Simulated Plastic Bonded Explosives*, in *Mechanical and Materials Engineering*. Washington State University, Washington (2011)

9. Wang, Z., et al.: Tensile mechanical properties and constitutive model for HTPB propellant at low temperature and high strain rate. *J. Appl. Polym. Sci.* **132**, 42104 (2015)
10. Renganathan, K., et al.: Tensile fracture of HTPB based propellant specimens. *Mater. Sci. Technol.* **18**(11), 1408–1412 (2013)
11. Xu, F., Aravas, N., Sofronis, P.: Constitutive modeling of solid propellant materials with evolving microstructural damage. *J. Mech. Phys. Solids*. **56**(5), 2050–2073 (2008)
12. Kalaycioglu, B., Dirikolu, M.H., Çelik, V.: An elasto-viscoplastic analysis of direct extrusion of a double base solid propellant. *Adv. Eng. Softw.* **41**(9), 1110–1114 (2010)
13. Trumel, H., et al.: A constitutive model for the dynamic and high-pressure behaviour of a propellant-like material: part II: model development and applications. *Int. J. Numer. Anal. Methods Geomech.* **25**(6), 581–603 (2001)
14. Trumel, H., et al.: A constitutive model for the dynamic and high-pressure behaviour of a propellant-like material: part I: experimental background and general structure of the model. *Int. J. Numer. Anal. Methods Geomech.* **25**(6), 551–579 (2001)
15. Trumel, H., Fanget, A., Deragon, A.: A finite strain elastic-plastic model for the quasi-static behaviour of particulate composites. *Int. J. Eng. Sci.* **34**(6), 677–698 (1996)
16. Tsai, J., Sun, C.T.: Constitutive model for high strain rate response of polymeric composites. *Compos. Sci. Technol.* **62**, 1289–1297 (2002)
17. Prakash, C., et al.: Strain rate dependent failure of interfaces examined via nanoimpact experiments. In: Antoun, B. et al. (eds.) *Challenges in Mechanics of Time Dependent Materials*, vol. 2. Conference Proceedings of the Society for Experimental Mechanics Series. Springer, Cham, pp. 93–102 (2017)
18. Verma, D., Tomar, V.: An investigation into environment dependent nanomechanical properties of shallow water shrimp (*Pandalus platyceros*) exoskeleton. *Mater. Sci. Eng. C Mater. Biol. Appl.* **44**, 371–379 (2014)
19. Verma, D., Tomar, V.: A comparison of nanoindentation creep deformation characteristics of hydrothermal vent shrimp (*Rimicaris exoculata*) and shallow water shrimp (*Pandalus platyceros*) exoskeletons. *J. Mater. Res.* **30**(08), 1110–1120 (2015)
20. Verma, D., Tomar, V.: An investigation into mechanical strength of exoskeleton of hydrothermal vent shrimp (*Rimicaris exoculata*) and shallow water shrimp (*Pandalus platyceros*) at elevated temperatures. *Mater. Sci. Eng. C Mater. Biol. Appl.* **49**, 243–250 (2015)
21. Verma, D., Qu, T., Tomar, V.: Scale dependence of the mechanical properties and microstructure of crustaceans thin films as biomimetic materials. *JOM.* **67**(4), 858–866 (2015)
22. Prakash, C., et al.: An analysis of the influence of grain boundary strength on microstructure dependent fracture in polycrystalline tungsten. *Int. J. Fract.* **199**(1), 1–20 (2016)
23. Fish, J., et al.: AL 6061-T6-Elastomer impact simulation. Technical Report. Rensselaer Polytechnic Institute (2005)
24. Hui, T., Oskay, C.: Computational modeling of polyurea-coated composites subjected to blast loads. *J. Compos. Mater.* **46**(18), 2167–2178 (2012)
25. Tomar, V.: Insights into the effects of tensile and compressive loadings on microstructure dependent fracture of trabecular bone. *Eng. Fract. Mech.* **76**(7), 884–897 (2009)
26. Ortiz, M., Pandolfi, A.: Finite-deformation irreversible cohesive elements for three-dimensional crack-propagation analysis. *Int. J. Numer. Methods Eng.* **44**(9), 1267–1282 (1999)
27. Tvergaard, V.: Cohesive zone representations of failure between elastic or rigid solids and ductile solids. *Eng. Fract. Mech.* **70**(14), 1859–1868 (2003)
28. Camacho, G.T., Ortiz, M.: Computational modeling of impact damage in brittle materials. *Int. J. Solids Struct.* **33**(20–22), 2899–2938 (1996)
29. Zhai, J., Tomar, V., Zhou, M.: Micromechanical simulation of dynamic fracture using the cohesive finite element method. *J. Eng. Mater. Technol.* **126**(2), 179 (2004)
30. Tomar, V., Zhai, J., Zhou, M.: Bounds for element size in a variable stiffness cohesive finite element model. *Int. J. Numer. Methods Eng.* **61**(11), 1894–1920 (2004)

Fracture, Fatigue, Failure and Damage Evolution,
Volume 7

Proceedings of the 2017 Annual Conference on
Experimental and Applied Mechanics

Carroll, J.; Shuman, X.; Beese, A.M.; Berke, R.B.; Pataky,
G.J. (Eds.)

2018, VIII, 127 p. 120 illus., 87 illus. in color., Hardcover
ISBN: 978-3-319-62830-1